HEFAT 2014
10th International Conference on Heat Transfer, Fluid Mechanics and Thermodynamics
14-16 July 2014
Orlando, Florida

ANALYSIS ON EFFECT OF SHAPES FOR MICROWAVE-ASSISTED FOOD PROCESSING OF 2D SAMPLES

Tanmay Basak*[a], S. Sriram[a], Soumen Panda[a], and Madhuchhanda Bhattacharya[b]

[a] *Department of Chemical Engineering, Indian Institute of Technology Madras, Chennai - 600036, India*
[b] *C2-5-4C, Delhi Avenue, Indian Institute of Technology Madras Campus, Chennai-600036, India*

Abstract

Present work provides guidelines on forecasting heating patterns in microwave processed foods which influence their final properties and quality. Three different cross-sections with equal area have been considered, namely, circular, square (indicated as Type 1) and square inclined at an angle of 45° with horizontal plane (indicated as Type 2). have been assumed to be exposed to lateral and radially incident microwaves. Microwave power absorption within samples have been studied using dimensionless parameters, viz. (i) N_w: represents the effect of sample size on power absorption. (ii) f_p and f_w: represents the effect of dielectric properties on power absorption Food materials were classified into 4 Groups with their f_p, f_w, as low f_p and low f_w (Group 1), low f_p and high f_w (Group 2), high f_p and low f_w (Group 3), high f_p and high f_w (Group 4), where low f_p (f_w) represents f_p (f_w)<0.3, while high f_p (f_w) represents f_p (f_w)≥0.3. Power and temperature profiles have been studied in representative materials from each Group. It is found that power absorption profiles for all groups of food and for all the shapes of circular, Type 1 and Type 2 occur in three regime in increasing order of sample size, i.e (i) thin regime: characterized by uniform power absorption (ii) intermediate regime: resonances in absorbed power and (iii) thick regime: exponential attenuation of power within sample. It is also found that, in general identical areas of all the three shapes give rise to identical power absorption at any given sample dimension. Formation and location of hot-spots within material is found to be dependent on the type of incidence, sample dimensions and cross-section of material.

Introduction

The innate advantage of volumetric heating offered by microwaves has largely been harnessed by food industries where, heating using conventional methods results in long processing times which further result in loss of vital components. Due to larger heating rates, microwaves have found successful applications in many food processing applications such as tempering, cooking, sterilization, drying, etc. [1–6]. However, microwave processed foods often do not have desired sensory attributes (in terms of color, taste, texture, etc.) due to phenomenon of non-uniform heating. Moreover, microwave processed foods also raises the issue of safety concerns as pathogens may survive in the regions of lower temperatures caused due to uneven heating [6, 7].

Microwave power absorption within materials at a given incident frequency, f, is governed by material dielectric properties, material shape and size. Mathematical characterization of power absorption features during microwave propagation within materials is performed using three length scales, namely, material dimension (length L or diameter D, based on the cross section of food material), wavelength of microwave within material (λ_m) and penetration depth of microwave within material (D_p defined as the distance at which which electric field decreases to 37% of its incident value). The length scales, λ_m and D_p are related to the dielectric properties (dielectric constant, κ' and dielectric loss, κ'') by the following expressions:

$$\lambda_m = \frac{c\sqrt{2}}{f\left[\sqrt{(\kappa')^2 + (\kappa'')^2} + \kappa'\right]^{1/2}}, \tag{1}$$

$$D_p = \frac{c}{\sqrt{2}\pi f\left[\sqrt{(\kappa')^2 + (\kappa'')^2} - \kappa'\right]^{1/2}}, \tag{2}$$

where c is the velocity of light and f is the frequency of incident radiation. Based on the relative magnitude of sample dimension compared to wavelength and penetration depth of the microwave within the material, the absorbed power can either be uniform or that can exhibit non-monotonic features such as local maxima across the sample (due to spatial resonances) or remain largely restricted to sample boundaries causing localized heating only at the edges [8]. Enhanced heating processes based on resonances and uniform heating within samples with minimal hot-spots for various food samples are critical issues which form the basis of current work. Despite significant experimental and modeling studies on power and temperature profiles in foods [6], a comprehensive analysis consisting of all possible food materials with wide range of sample dimensions and the possible effect of shapes is yet to appear in literature.

In this work, we consider three different cross-sections of 2D food materials with identical area as shown in Fig. 1. Three different cross-sections are selected as circular, square (Type 1) and square inclined at an angle of 45° with horizontal plane (Type 2). These cross-sections have been chosen based on commonly encountered foods such as bread

*Corresponding author:tanmay@iitm.ac.in

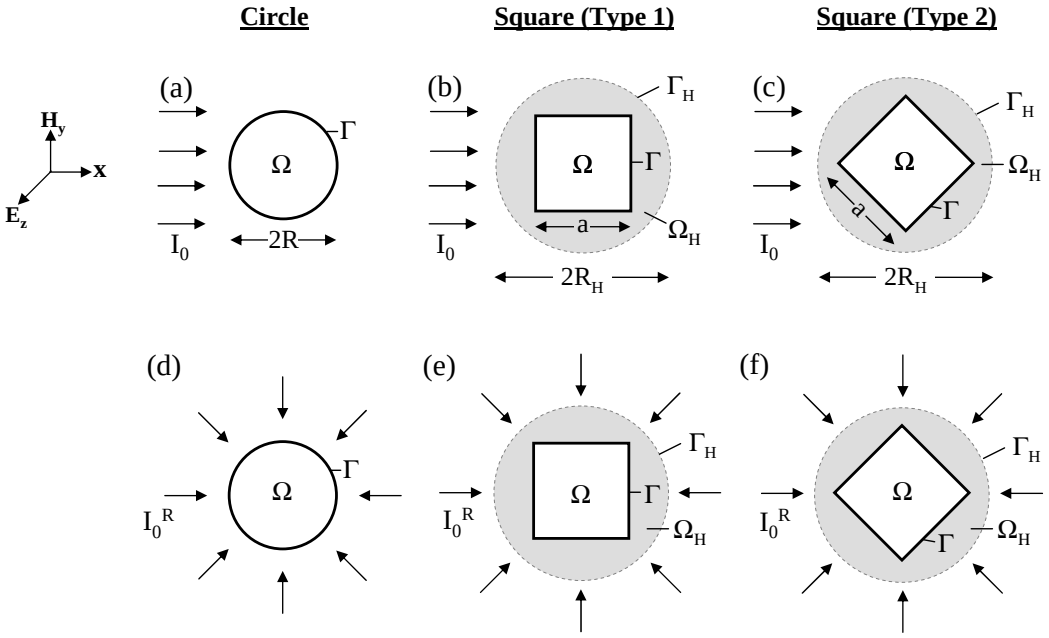

Figure 1: Configurations of lateral (a-c) and radial (d-f) irradiations on circular and square (Type 1 and Type 2) food samples.

slices, meat rolls, sausages, vegetables, etc. Food materials with the above cross-sections are assumed to be exposed to lateral [Fig. 1(a)-(c)] and radial [Fig. 1(d)-(f)] irradiations of microwaves [9–12] of intensities I_0 and I_0^R, respectively. It may be noted that the situation of lateral irradiations in Fig. 1(a)-(c) become equivalent to the cases of Fig. 1(d)-(f) if the samples rotate around their major axis (along z direction) [1]. However, this equivalence between lateral and radial irradiations is maintained if their intensities satisfy the relation of $I_0^R = I_0/4$ to match the induced electric field in cases of infinitesimally small samples, where electric field becomes invariant of the position and hence rotation of the sample [11, 12]. Note that, in the limit of infinitesimally small samples: Eqns. 18-20 of reference [11] or Eqns. 20-22 of reference [12] result in $E_m \rightarrow 2E_0^R$, while Eqns. 13-17 of reference [11] or Eqns. 15-19 of reference [12] lead to $E_m \rightarrow E_0$ for lateral incidence. Since $E_0 = \sqrt{2I_0/c\epsilon_0}$ and $E_0^R = \sqrt{2I_0^R/c\epsilon_0}$ with ϵ_0 as the free space permittivity, the following relationships given by $E_0^R = E_0/2$ or $I_0^R = I_0/4$ must be maintained to satisfy the same induced electric field for lateral and radial irradiations in the limit of infinitesimally small samples. Hence, we will consider $I_0^R = I_0/4$ in all the simulations to perform a comparative analysis between the two radiation schemes. In this work, we have assumed $I_0 = 1$ W/cm^2 corresponding to $I_0^R = 0.25$ W/cm^2.

The influence of sample size and dielectric properties on power absorption characteristics are carried out using three dimensionless parameters, namely N_w, f_p and f_w, defined as [13, 14]

$$N_w = \frac{2R}{\lambda_m}, \quad f_p = \frac{\lambda_m}{2\pi D_p}, \quad \text{and } f_w = \frac{\lambda_m}{\lambda_0} \ , \qquad (3)$$

where R is the radius of the circular samples and $\lambda_0 = c/f$ is the wavelength of microwave within the surrounding free space. Being the ratio of $2R$ and λ_m, wave number, N_w represents the effect of sample dimensions for circular as well as square samples since their dimensions are interrelated as $R = a/\sqrt{\pi}$ following equal area ($\pi R^2 = a^2$) [It may be noted that wave number can also be defined with respect to the dimension of square samples as $N_{w,s} = a/\lambda_m$, but we represent the results in terms of N_w and the corresponding wave number or sample dimension for square samples ($N_{w,s}$) can be easily obtained from the above relations.]. Parameters f_p and f_w represent relative magnitudes of microwave wavelength within the sample compared to the penetration depth of the sample and microwave wavelength within the surrounding free space, respectively and they capture the variations of dielectric properties of the material. The advantage of operating in the f_p-f_w scale instead of λ_m-D_p scale is that both f_p and f_w are bounded between 0 and 1 (from definition of Eqns. 1 and 2 and the fact that $\lambda_0 \geqslant \lambda_m$) compared to unboundedness of λ_m and D_p for all probable food materials. Thus, variation of f_p and f_w from 0 to 1 would ensure encompassment of all food materials.

Microwave power absorption within various cross sections have been obtained via solution of Helmholtz or wave equation for induced electric field and heating characteristics are obtained via solution of energy balance equation as outlined below. Generalized heating patterns in all possible food materials are provided by grouping foods based on their f_p and f_w values (as shown in Tables 1-4) and with a representative study from each group. The rationale behind such a grouping will be discussed later in this paper.

Governing Equations: power and temperature distributions

With the assumption of constant dielectric properties, the governing wave equation describing the induced electric field within the sample (E_m) becomes invariant of the local temperature and can be written in terms of N_w, f_p and f_w

Table 1: Group 1: Low f_p, low f_w.

Material	$\kappa^{'}$	$\kappa^{''}$	λ_m (m)	D_p (m)	f_p	f_w
Apple [15]	54	10	0.0166	0.0288	0.0918	0.1355
Banana [15]	60	18	0.0156	0.0170	0.1468	0.1277
Carrot [15]	56	15	0.0162	0.0196	0.1316	0.1325
Cucumber [15]	69	12	0.0147	0.0271	0.0863	0.1199
Grapes [15]	65	17	0.0151	0.0186	0.1286	0.1230
Orange [15]	69	16	0.0146	0.0204	0.1144	0.1196
Papaya [15]	67	14	0.0149	0.0229	0.1034	0.1215
Peach [15]	67	14	0.0149	0.0229	0.1034	0.1215
Potato [15]	57	17	0.0160	0.0175	0.1459	0.1310
Strawberry [15]	71	14	0.0145	0.0236	0.0977	0.1181
Beef (forequater trimmings) [16]	43.7	13.7	0.0183	0.0190	0.1531	0.1495
Lamb (leg) [16]	49.4	15	0.0172	0.0185	0.1485	0.1407
Chicken (breast) [16]	49	16.1	0.0173	0.0172	0.1601	0.1410
Shrimp [10]	61.4	31.4	0.0152	0.0100	0.2409	0.1239
Pork Luncheon Roll (PLR) [17]	35.9	18.03	0.0199	0.0133	0.2370	0.1621
Beef (cooked) [18]	30.5	9.60	0.0219	0.0227	0.1537	0.1789
Cooked macaroni noodles (915) [19]	30.05	4.15	0.0597	0.1382	0.0687	0.1820

Table 2: Group 2: Low f_p, high f_w.

Material	$\kappa^{'}$	$\kappa^{''}$	λ_m (m)	D_p (m)	f_p	f_w
Bread (2800) [18]	4.6	0.6	0.0499	0.1222	0.0649	0.4653
Potato, freeze dried (3000) [18]	7.5	2.5	0.0360	0.0353	0.1623	0.3603
Oil [13]	2.8	0.15	0.0732	0.4350	0.0268	0.5974

as [12, 13]

$$\nabla^2 E_m + \pi^2 N_w^2 \left(1 + i f_p\right)^2 E_m = 0,\ x, y \in \Omega \tag{4}$$

where ∇^2 is the dimensionless Laplacian operator in domain Ω scaled with radius of the circular sample. The boundary conditions associated with the above equations require to consider scattering of microwaves from the outer surface of the samples and for non-circular samples, boundary conditions can be expressed in closed-form by considering a hypothetical circular surface around the sample [12] as shown in Fig. 1(b)-(c) and (e)-(f) (denoted as Ω_H). In such cases, determination of electric field requires to solve additional wave equation in domain Ω_H given by

$$\nabla^2 E_H + \pi^2 N_w^2 f_w^2 E_H = 0,\ x, y \in \Omega_H \tag{5}$$

in conjunction with that in domain Ω given in Eqn. 4 and continuity of electric and magnetic field at the interface Γ given by

$$@\,\Gamma:\ \{E_H = E_m,\ \ \boldsymbol{n} \cdot \boldsymbol{\nabla} E_H = \boldsymbol{n} \cdot \boldsymbol{\nabla} E_m\ , \tag{6}$$

where $\boldsymbol{n}$ is the outward normal to surface Γ and $\boldsymbol{\nabla}$ is the gradient operator. The additional radiation boundary conditions at hypothetical surface (Γ_H) for lateral and radial irradiations are given by

$$\mathbf{n} \cdot \boldsymbol{\nabla} E_H|_{\Gamma_H} = \begin{cases} \pi N_w f_w \sum_{n=0}^{\infty} \Bigg[E_0 \epsilon_n i^n \Bigg(J_n'(\beta) \\ -J_n(\beta) \dfrac{H_n^{(1)'}(\beta)}{H_n^{(1)}(\beta)} \Bigg) \cos\left[n\phi\right] + \dfrac{\epsilon_n H_n^{(1)'}(\beta)}{2\pi H_n^{(1)}(\beta)} \\ \times \displaystyle\int_0^{2\pi} E_H|_{\Gamma_H} \cos\left[n(\phi - \phi')\right] d\phi' \Bigg], \text{lateral} \\ -\pi N_w f_w \left(\dfrac{2iE_0}{\pi\beta H_0^{(1)}(\beta)} + \dfrac{H_1^{(1)}(\beta)}{H_0^{(1)}(\beta)} E_H|_{\Gamma_H} \right), \\ \text{radial} \end{cases} \tag{7}$$

where,

$$\epsilon_n = \begin{cases} 1 & \text{for } n = 0 \\ 2 & \text{otherwise} \end{cases} \quad \text{and} \quad \beta = \pi N_w f_w \frac{R_H}{R}. \tag{8}$$

The same procedure can also be followed for circular samples. Alternatively, Eqn. 4 can be directly solved using the radiation boundary conditions at the sample surface (Γ) without the solution of Eqn. 5 in which case β simplifies to $\beta = \pi N_w f_w$.

Once the electric field is obtained, absorbed microwave power (q) is deduced using the following expression:

$$q = \frac{2\pi c \epsilon_0 f_p}{f_w^2 \lambda_0} E_m E_m^*, \tag{9}$$

where E_m^* is the complex conjugate of E_m. The overall heating rate is quantified by average power given by the following [11]:

$$q_{avg} = \frac{1}{A_c} \iint_{\Omega} q(\Omega) d\Omega, \tag{10}$$

where A_c is the cross-section of food material. Corresponding evolution of temperature (T) within the material is simulated from the following energy balance equation, boundary and initial conditions:

$$\rho c_p \frac{\partial T}{\partial t} = k \nabla^2 T + q;\ \ \begin{cases} @\Gamma : \mathbf{n} \cdot k \nabla T = 0 \\ @t = 0 : T = T_0 \end{cases}, \tag{11}$$

which assume the sample to be at uniform temperature of $T_0 = 300$K at the beginning of the process and the surface of the sample to be thermally insulated. In Eqn. 11, ρ is the density, c_p is the specific heat, k is the thermal conductivity and t is the time. Wave equations (Eqns. 4, 5) and energy balance equation (Eq. 11) are simultaneously solved using a robust in-house code involving Galerkin finite element method for space discretization and Crank-Nicholson

Table 3: Group 3: High f_p, low f_w.

Material	κ'	κ''	λ_m (m)	D_p (m)	f_p	f_w
White Pudding (WP) [17]	32.83	23.09	0.0203	0.0102	0.3164	0.1656
Frankfurters (2800) [18]	39.0	26.9	0.0163	0.0083	0.3114	0.1522
Ham (2800) [18]	66.6	47.00	0.0125	0.0062	0.3173	0.1162
Whey protein mixture (915) [19]	60.40	38.25	0.0404	0.0222	0.2900	0.1231

Table 4: Group 4: High f_p, high f_w.

Material	κ'	κ''	λ_m (m)	D_p (m)	f_p	f_w
Peanut butter (2800) [18]	3.1	4.10	0.0528	0.0169	0.4976	0.4927
Almonds (915) [16]	3.2	6.4	0.1441	0.0371	0.6180	0.4395
Walnut (915) [16]	2.1	2.6	0.1988	0.0662	0.4778	0.6062

scheme for time integration (see [11] and [12] for full mathematical treatment). In all the simulations, we have used $2R_H/a = 2$, following an earlier work [12]. Finally, the average temperature ($\overline{T}$) is obtained by integrating Eqn. 11 over the material cross-section.

Results and Discussions

Preliminary analysis was carried out on the variation of q_{avg} with sample size by varying f_p from 0.01 to 1 at certain fixed f_w values and by varying f_w from 0.01 to 1 at fixed f_p values for both lateral and radial incidences (figures not shown). It was observed that the magnitudes of f_p and f_w strongly influence resonances in absorbed power. Note that, hotspots within samples arise as a consequence of resonances and multiple resonating peaks lead to multiple zones of hotspots. Further, it was observed that the resonances in power were found to be more pronounced with decreasing f_p values and those are gradually reduced with increasing f_p values. At around $f_p \geq 0.3$, resonances for both types of incidences are found to disappear. Similar effects were observed with f_w, where resonating features were found to diminish as f_w approaches 1. Thus, the grouping of food materials based on high and low f_p (f_w) values have been chosen with f_p (f_w)=0.3 and the four combinations presented here would ensure coverage of all food materials.

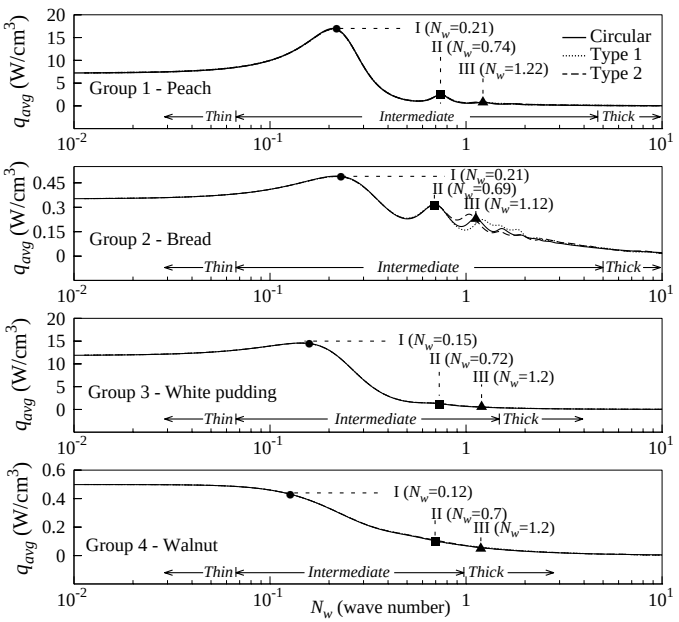

Figure 2a: Average power as a function of sample size for representative materials from Group 1-4 due to lateral incidence of food samples samples with circular and square cross-sections.

Average power distributions

Average absorbed power as a function of dimensionless sample size (N_w) within various food materials, representative of each group (Group 1: peach; Group 2: bread; Group 3: white pudding; Group 4: walnut) for lateral and radial incidences are shown in Figs. 2a and 2b, respectively. The effect of shape on average power during lateral incidence is shown using solid (for circle), dotted (for Type 1) and dashed (for Type 2) lines. Features of radial incidence on square samples remain invariant of the orientation (Type 1 and Type 2), as the sample is exposed to microwaves at all points (see Fig. 1 (e)-(f)). Thus, the analysis of power and temperature are shown for Type 1 only for radial incidence, as simulations with Type 2 give identical features with those of Type 1.

Figures 2a and 2b illustrate that, power absorption profiles for any material and any shape can be divided into 3 regimes as (i) *thin* regime (sample dimension much smaller than wavelength of microwave), characterized by uniform power absorption, (ii) *thick* regime (sample dimension much greater than penetration depth), where absorbed power attenuates quickly within samples and (iii) *intermediate* regime, which may either exhibit non-monotonic (for Groups 1 and 2) or monotonic (for Groups 3 and 4) based on f_p, f_w values. It is interesting to note that for all groups of food materials of any shape, $N_w \lesssim 0.1$ correspond to *thin* regime and $2\pi N_w f_p \equiv N_p \gtrsim 3$ correspond to *thick* regime. In accordance with the limit $N_p \equiv 2\pi N_w f_p \lesssim 3$ for the *intermediate regime*, it is observed from Figs. 2a and 2b that smaller values of f_p corresponding to Group 1 and 2 lead to the *intermediate* regime to span over a larger range of sample dimensions with multiple resonating peaks compared to Group 3 and 4 which show monotonic decrease from *thin* to *thick* regime due to higher values of f_p. Further, it is observed that the resonating features are more prominent for lateral incidence compared to radial incidence, where lateral incidence leads to additional maxima in average power for

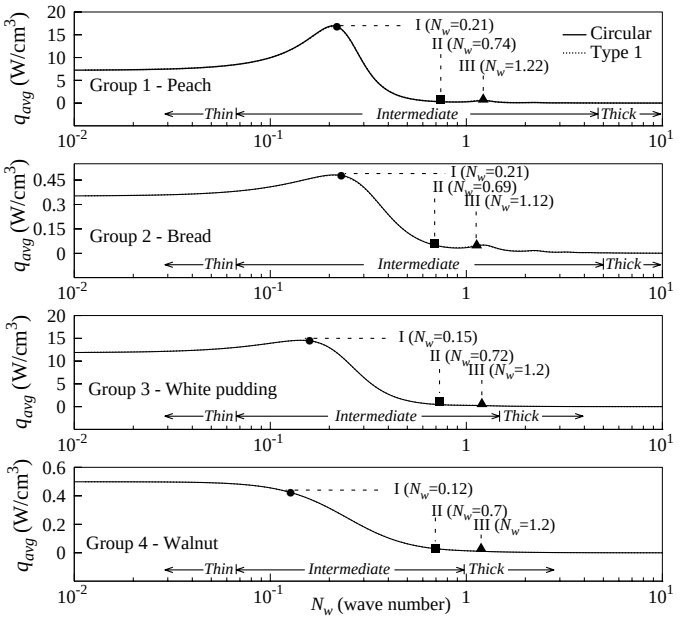

Figure 2b: Average power as a function of sample size for representative materials from Group 1-4 due to radial incidence of food samples samples with circular and square cross-sections.

food materials belonging to Group 1 and 2. (see Fig. 2a and 2b). Specific sample dimensions have been identified in Figs. 2a and 2b as regime I (shown by bullets), regime II (shown by filled squares) and regime III (shown by filled triangles) in the increasing order of sample dimensions (N_w) to perform a comparative analysis based on spatial distribution of power and temperature between the two schemes of lateral and radial irradiations. Note that, regimes I, II and III correspond to the first three resonating peaks for laterally incident Group 1 and 2 food materials (see Fig. 2a). The sample dimensions have been chosen beyond the *thin* regime due to the fact that *thin* regime is invariant of incidence type and that corresponds to uniform power absorption without the occurrence of hot-spots.

Figures 2a and 2b further illustrate that, in general, identical areas of circle, Type 1 and Type 2 cross-sections give rise to identical power absorption values at any given sample dimension and incidence type for all food materials (Group 1-4) except for few N_w values for Group 2 materials during lateral irradiation beyond Regime II. It is observed that the average powers at regime I (corresponds to maxima in power for both lateral and radial) for Group 1 and Group 3 materials are around 15 and 13 W cm^{-3}, respectively while the average powers are around 0.45 and 0.4 W cm^{-3} for Group 2 and Group 4 materials, respectively for both lateral and radial incidences. At regime II (corresponds to maxima for lateral and minima for radial) it is observed that the average powers for Group 1 and 3 are around 2.5 and 1 W cm^{-3}, respectively while the average power for Group 2 and 4 are around 0.3 and 0.1 W cm^{-3}, respectively for lateral incidence. On the other hand the average power at regime II during radial incidence is around 0.7 and 0.9 W cm^{-3} for Group 1 and 3, respectively while the average powers are around 0.05 and 0.03 W cm^{-3} for Group 2 and 4, respectively. Regime III corresponds to maxima in power for both lateral and radial incidences and is a representative dimension within a upper limit of *intermediate* or in *thick* regime (for Group 4). It is observed that the average powers are around 0.75 and 0.6 W cm^{-3}, for Group 1 and 3, respectively while they are around around 0.23 and 0.05 W cm^{-3} for Group 2 and 4, respectively for lateral incidence. Note that, the average power corresponding to Type 2 in regime III is slightly higher compared to the other two configurations (see Fig. 2a). In contrast, the average power is around 0.75 and 0.6 W cm^{-3} for Group 1 and Group 3, respectively while they are around 0.05 and 0.03 W cm^{-3} for Group 2 and Group 4, respectively for radial incidence. Thus, it can be inferred that the differences in power absorption between lateral and radial become prominent for Group 2 and Group 4 (high f_w) materials (see Fig. 2a and 2b). Further, it is observed that the overall magnitudes of absorbed power are very less for Group 2 and Group 4 (high f_w) materials which imply their poor heating rates. While the average power at the selected regimes gives an overall idea about the heating rates, spatial distribution of power and temperature are important for critical issues such as thermal runaway, which are discussed next.

Power and temperature profiles

The thermal properties of materials used for the temperature studies are reported in Table 5. Due to lack of data for thermal conductivity data for walnuts, the thermal conductivity data of cashew was used. It may be noted that the above assumption may not affect the results, as the power absorption features depend on dielectric properties and the order of magnitudes of thermal conductivities of foods are nearly similar [24, 26]. In general, the processing time was fixed at 120 s. However, due to faster heating rates by Group 1 and 3 due to their high magnitude of absorbed power, simulation studies showed a high shoot up of temperature (of the order of 1000°C) and due to low power absorption by Group 2 and 4, insignificant temperature rise was observed. Hence, the temperature set points were fixed as: 310 K$\leq T\leq$ 400 K (as vaporization of moisture would occur beyond 400 K) and the processing time of 120 s was fixed subject to the above set-points. If the temperature falls outside the set-points, a lower or higher value of time is used correspondingly.

Figs. 3a-c show the power and temperature distributions for lateral incidence at sample dimensions corresponding to regime I, where sub-figures (a), (b) and (c) denote distributions for circle, Type 1 and Type 2, respectively. Regime I is characterized by the occurrence of single maxima in power near the centre for Group 1 and Group 3 materials and near the unexposed face for Group 2 and Group 4 materials for circle, Type 1 and Type 2 cross-sections. Note that, these maxima occur due to constructive interference of travelling waves within the sample. It is observed that the maxima in spatial power for Group 1 material (peach) are around 18.5 W cm^{-3} while Group 2 (bread), 3 (white pudding), 4 (walnut) show maxima of corresponding to 0.56, 15.2 and 0.45 W cm^{-3}, respectively for all the cross-sections of circle, Type 1 and Type 2. It is interesting to note that Group 1 and Group 3 correspond to power maxima with larger and similar order of magnitudes corresponding to lower f_w values, whereas Group 2 and Group 4 materials show smaller values of power maxima with higher f_w values. Corresponding to power maxima, maxima in temperatures occur near the

Table 5: Thermal properties of materials used in temperature calculations.

Material	ρ (kg/m^3)	C_p (J/kgK)	k (W/mK)
Peach	769 [20]	3,770 [21]	0.5815 [21]
Bread	800 [18]	2850 [18]	0.450 [18]
White Pudding (WP)	931.88 [22]	3,331 [17]	0.35 [17]
Walnut	528 [23]	209 [24]	0.23 [25]

unexposed face for circle, Type 1 and Type 2 cross-sections. The average temperature values ($\overline{T}$) for Group 2 and Group 4 materials are lower compared to Group 1 and Group 3 (the maxima in temperature reaches around 400 K in 20 s) due to lower power absorption by Group 2 and 4 materials (see Fig. 2a). The temperature difference (ΔT) which is defined as the difference between maximum temperature and minimum temperature within samples denotes the extent of thermal runaway. It is observed from Figs. 3a-c that ΔT values are around 3-4 K for all the cross-sections, indicating no significant thermal runaway. The spatial power and temperature profiles further reveal that there is no significant effect of shape at regime I.

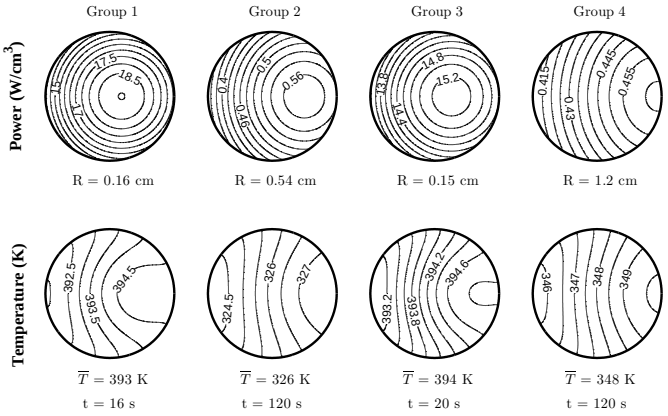

Figure 3a: Power and temperature profiles for food materials from Group 1-4 at sample radius corresponding to regime I for laterally irradiated circular samples.

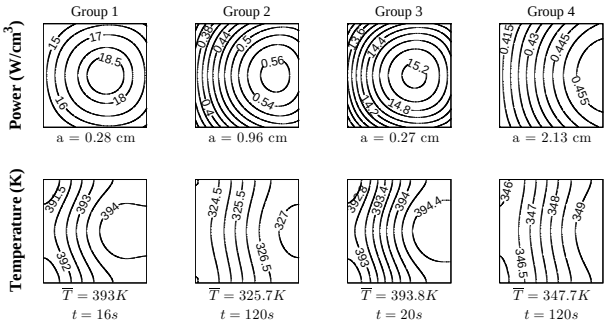

Figure 3b: Power and temperature profiles for food materials from Group 1-4 at sample radius corresponding to regime I for laterally irradiated Type 1 samples

Figures 4a-c show the power and temperature distributions for lateral incidence corresponding to regime II where the sub-figures (a), (b) and (c) denote distributions for circle, Type 1 and Type 2 respectively. Regime II shows the presence of multiple maxima for all groups of food and

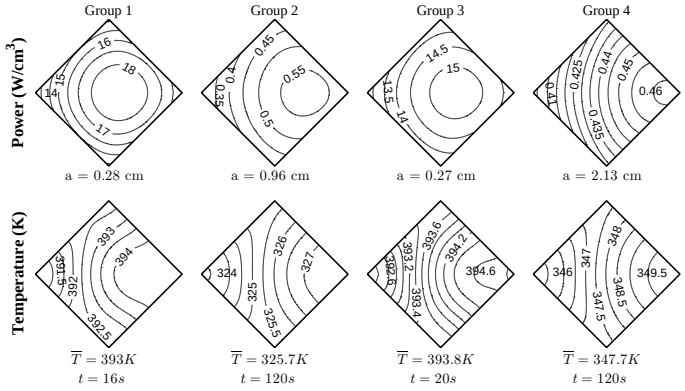

Figure 3c: Power and temperature profiles for food materials from Group 1-4 at sample radius corresponding to regime I for laterally irradiated Type 2 samples.

for all the three cross-sections implying that larger sample dimensions favour more resonances in the *intermediate* regime. Food materials belonging to Group 1-3 of circular and Type 1 configuration show a primary maxima at the opposite face and a secondary maxima at the incident face. Type 2 cross-section of Group 1 and 2 materials show primary and secondary maxima at the right and left corners along the direction of wave propagation, respectively while Type 2 cross-section of Group 3 material show primary maxima at the left incident corner and secondary maxima at the right corner. The high f_p values of Group 4 shifts the location of primary maxima to the exposed face for circle and Type 1 and to the left corner for Type 2. It is observed that the magnitude of primary maxima for Group 1 material with circle and Type 1 cross-sections are around 6 W cm^{-3}, while secondary maxima are around 4 W cm^{-3}, for circle and Type 1. It is also observed that Type 2 configurations of Group 1 give rise to a slightly higher primary maxima of around 7 W cm^{-3}, around the right corner. Similar to power absorption features, Group 1 shows a primary maxima in temperature (415 K) at the opposite face for circle and Type 1, while secondary maxima of around 385 K occurs at the incident face for circle and Type 1. Group 1 material of Type 2 cross-sections, corresponding to their higher power maxima, shows a higher value of maxima in temperature of around 430 K (primary) and 400 K (secondary) at the right and left corners respectively. Magnitudes of primary maxima in power for Group 3 materials for circle and Type 1 are around 2.5 W cm^{-3} (right face) 2.0 W cm^{-3} (left face), respectively while Type 2 shows a primary maxima of around 3 W cm^{-3} (left corner) and secondary maxima of around 2.5 W cm^{-3} (right corner). Correspondingly, a primary maxima in temperature (365 K) at the right face and another local maxima (360 K) at left face occur for circle and Type 1 configurations of Group 3 materials. On the other hand, Type 2 configu-

ration corresponds to a to a primary maxima (≈380 K) at the left corner while another local maxima (≈370 K) occur at the right corner. The magnitudes of maxima for Group 2 and 4 are very much low compared to Group 1 and 3. Thermal runaway in regime II (measured by ΔT values) is very prominent and it is observed that Group 1 shows ΔT value of around 35-40 K for circle and Type 1 while Type 2 shows ΔT value of around 60 K. Similarly, ΔT values for Group 3 material is around 25-30 K for circle and Type 1 while Type 2 shows a thermal runaway of around 50 K. Group 2 and Group 4 show ΔT values of around 20-35 K for all the three cross-sections. It is interesting to note the effect of shape for Group 3 materials in regime II, where the primary maxima in power and temperature occur at the opposite face for circle and Type 1 while that occurs at the exposed face for Type 2 configurations. The effect of corner points are significant in regime II in materials with Type 2 cross-sections, where the different corner points are either primary or secondary hot spots or even regions of cold spots. (see Fig. 4c). Type 2 configurations exhibit severe runaway compared to circle and Type 1 but they offer the potential advantage of selective/targeted processing.

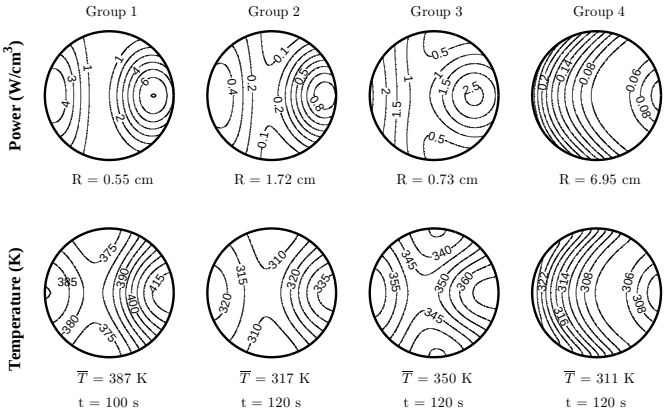

Figure 4a: Power and temperature profiles for food materials from Group 1-4 at sample radius corresponding to regime II for laterally irradiated circular samples.

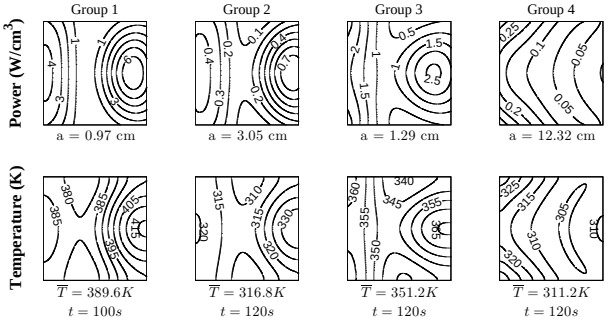

Figure 4b: Power and temperature profiles for food materials from Group 1-4 at sample radius corresponding to regime II for laterally irradiated Type 1 samples.

Figures 5a-c show the power and temperature distributions for lateral incidence corresponding to regime III. It is interesting to note that the location of primary maxima for Group 1 materials shifts from the opposite faces/corners to the center for all 3 configurations with a magnitude of

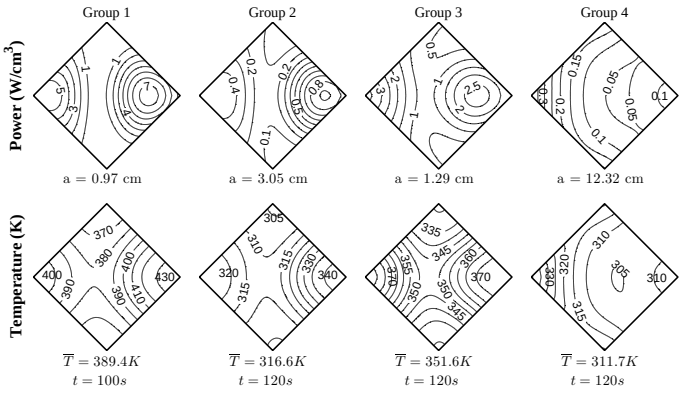

Figure 4c: Power and temperature profiles for food materials from Group 1-4 at sample radius corresponding to regime II for laterally irradiated Type 2 samples.

around 3 W cm^{-3}. Further, it is also interesting to note the role of corner points which lead to a secondary maxima of magnitude around 1.5 W cm^{-3} at the top and bottom corners of incident face in Type 1 and at left, top and bottom corners in Type 2 for Group 1 materials. The primary maxima in Group 2 (high f_w) material of magnitude 0.7 W cm^{-3} remains restricted at the opposite or right face for circular and Type 1 cross-sections and at the right corner for Type 2 cross-section. Materials corresponding to Group 3 with circular cross-sections show the development of primary maxima at the exposed face and a secondary maxima near the center with magnitudes of 1 and 0.6 W cm^{-3}, respectively. However, primary maxima for Group 3 materials occur near the top and bottom corners of left incident face for Type 1 (magnitude of around 1.8 W cm^{-3}) and at the left corner for Type 2 cross-sections (magnitude of around 2 W cm^{-3}. Additional secondary maxima of around 0.6 W cm^{-3} occur near the center (closer to right face) for Type 1 and at the top and bottom corners (of magnitude 1 W cm^{-3}) for Type 2 cross-sections. Interestingly, Type 2 cross-sections leads to an additional tertiary maxima which occurs near the center of sample. On the other hand, maxima in power for Group 4 materials occur near the exposed face for circular/Type 1 cross-sections and at the left corner for Type 2 cross-sections and the absorbed power is found to decrease monotonically within the sample. Features of temperature distributions qualitatively follow the trend of power distributions and the locations of maxima in temperature correspond to those of maxima in power. Significant thermal runaway is observed based on the ranges of spatial temperature (ΔT). It is observed that temperature varies within 326-346, 305-330 K for Group 1 and Group 2 materials, respectively with all the three cross-sections. Similarly, the variation of temperature is around 310-335 K for Group 3 materials with circular cross-sections. Type 1 and Type 2 cross-sections of Group 3 materials show variation in temperature of around 310-350 K and it is found that the corners get heated rapidly compared to sample interior. Heating occurs mostly from the incident face (in circle and Type 1) /left corners (Type 2) for Group 4 materials with temperature variation of around 305-340 K. Targeted/selective processing at the corner points in regime III can be achieved with both Type 1 and Type 2 cross-section which contrasts regime II, where only Type 2 cross-sections correspond to selective heating near the cor-

ners.

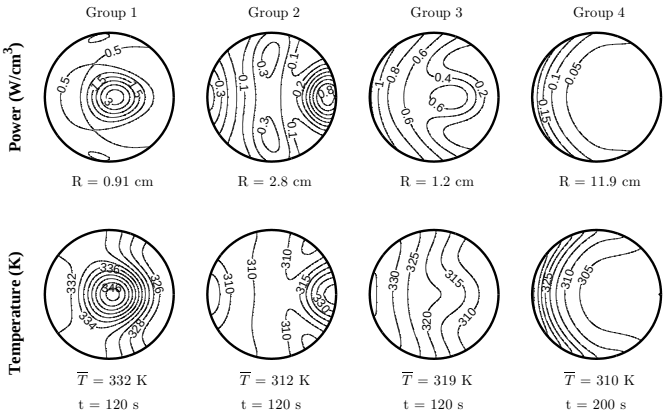

Figure 5a: Power and temperature profiles for food materials from Group 1-4 at sample radius corresponding to regime III for laterally irradiated circular samples.

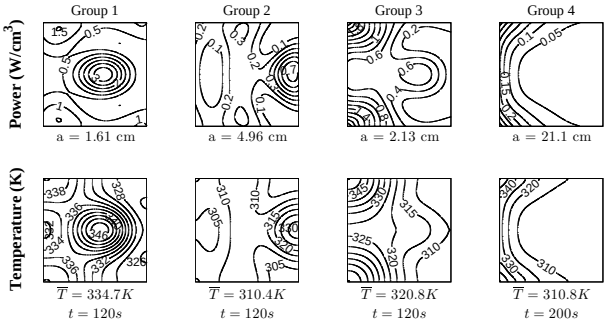

Figure 5b: Power and temperature profiles for food materials from Group 1-4 at sample radius corresponding to regime III for laterally irradiated Type 1 samples.

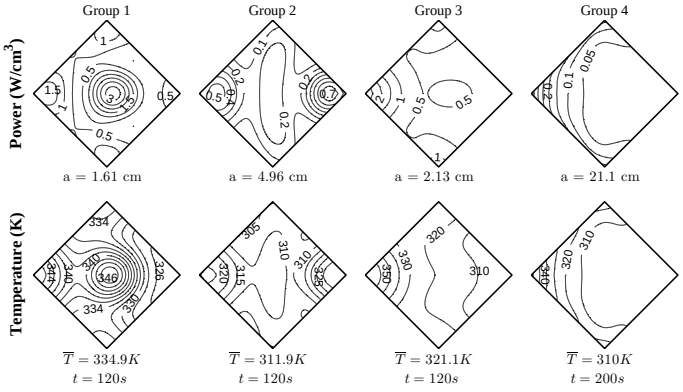

Figure 5c: Power and temperature profiles for food materials from Group 1-4 at sample radius corresponding to regime III for laterally irradiated Type 2 samples.

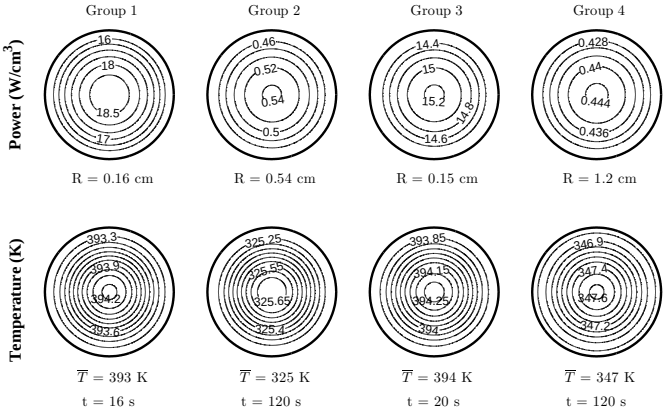

Figure 6a: Power and temperature profiles for food materials from Group 1-4 at sample radius corresponding to regime I for radially irradiated circular samples.

Figures 6a and 6b show power and temperature distributions for radial incidence at regime I, where lateral and radial incidence show similar power absorption. It is observed that maxima in power and temperature occurs at the center for circle and Type 1 which contrast the location of maxima at the opposite face for lateral incidence (see Fig. 3a-c). Note that, the corner points correspond to minima in temperature for square cross-sections. Magnitudes of maxima in power and temperature are similar to that of the corresponding laterally irradiated food samples. Due to similar magnitudes of absorbed power, the overall heating rates due to lateral and radial incidences are similar (see Figs. 2a and 2b). It is also observed that thermal runaway is almost negligible which indicates almost uniform heating.

Figures 7a and 7b show power and temperature distributions for radial incidence at regime II, where radial incidence shows lesser power absorption compared to lateral incidence (see Figs. 2a and 2b). In contrast to lateral incidence which shows multiple maxima, radial incidence shows only a single maxima at the center which suggest that radial incidence increases uniformity. The magnitudes of maxima are much lower compared to lateral incidence (at regime II) implying that radial incidence corresponds to poor heating rates in regime II. However, the ΔT values are much less (within 10 K) for all groups of food with circular and square shape.

Figures 8a and 8b show power and temperature distributions for radial incidence at regime III, where lateral and radial incidences show similar magnitudes of power absorption for Group 1 and different magnitudes of power absorption for Group 2, Group 3 and Group 4 materials (see Figs. 2a and 2b). It is observed that primary maxima in power occurs at the center and additional secondary maxima occurs near periphery for materials of Groups 1-4 with circular cross-sections. On the other hand, Type 1 cross-sections give rise to primary maxima at the center for all Groups except Group 4, where it occurs at the corner points. Note that, the magnitudes of primary maxima are 3, 0.25, 0.55 and 0.02 W cm^{-3} for Groups 1-4, respectively. The magnitudes of maxima in power for radial incidences are similar to lateral incidence for Group 1, while Group 2, 3 and 4 show comparatively lower values of maxima. The spatial temperature distributions follow similar trend as power distributions. It is observed that, during radial incidence maxima in temperatures of around 336, 326, 316 and 311 K occurs at the center for samples of Groups 1, 2 ,3 and 4, respectively with circular and Type 1 cross-sections. The thermal runaway values for Group 1 and Group 2 material are around 15-16 K. Similarly, the ΔT values of Group 3 and 4 are around 8-10 K. It is interesting to note that, radial irradiation of Type 1 cross-sections at all sample regimes gives rise to power and temperature distributions which are found to be radial functions near the

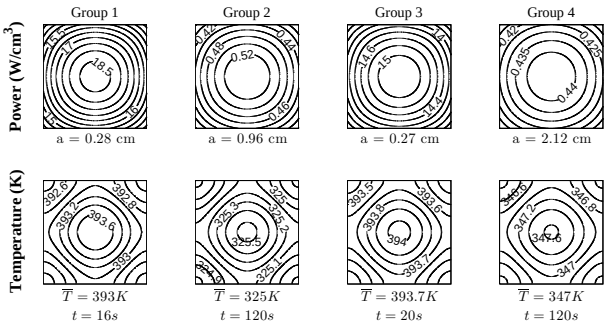

Figure 6b: Power and temperature profiles for food materials from Group 1-4 at sample radius corresponding to regime I for radially irradiated square (Type 1 or Type 2) samples.

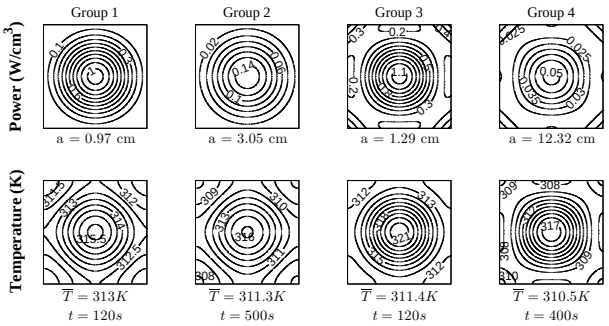

Figure 7b: Power and temperature profiles for food materials from Group 1-4 at sample radius corresponding to regime II for radially irradiated square (Type 1 or Type 2) samples.

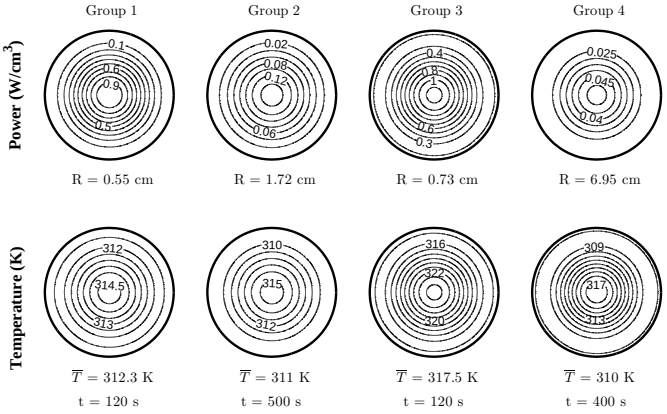

Figure 7a: Power and temperature profiles for food materials from Group 1-4 at sample radius corresponding to regime II for radially irradiated circular samples

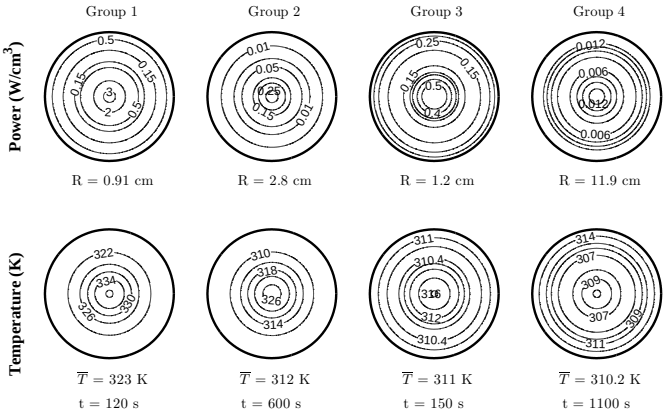

Figure 8a: Power and temperature profiles for food materials from Group 1-4 at sample radius corresponding to regime III for radially irradiated circular samples.

sample center.

Conclusion

This work is devoted to the analysis on the effect of shapes for processing of 2D samples and forecasting heating patterns within food materials. Three different cross-sections with equal area have been considered, namely, circular, square (indicated as Type 1) and square inclined at an angle of 45° with horizontal plane (indicated as Type 2) which are assumed to be exposed to lateral and radially incident microwaves. Microwave power has been deduced from Helmholtz equations using dimensionless parameters, namely, $f_p = \lambda_m/2\pi D_p$, $f_w = \lambda_m/\lambda_0$ and $N_w = D/\lambda_m$, where f_p and f_w relates to the effect of dielectric properties and N_w shows the effect of sample size. Based on f_p and f_w values, food materials were grouped into 4 categories as: low f_p and low f_w (Group 1, e.g. peach)), low f_p and high f_w (Group 2, e.g. bread), high f_p and low f_w (Group 3, e.g. white pudding), high f_p and high f_w (Group 4, e.g. walnut), where the low f_p (f_w) values refer to f_p (f_w)< 0.3 and high f_p (f_w) values refer to f_p (f_w)≥ 0.3. It is found that power absorption follows three distinct regimes which appear in increasing order of sample dimensions, namely, (i) *thin* regime: characterized by uniform power absorption (ii) *intermediate* regime: resonances in power absorption and *thick* regime: exponential attenuation of absorbed power within samples. Specific sample dimensions have been identified as regime I ($N_w \approx 0.2$), regime II ($N_w \approx 0.7$) and regime III ($N_w \approx 1.2$) for performing a comparative analysis between the two schemes of radiation. It is also observed that, in general, identical areas of circle, Type 1 and Type 2 cross-sections give rise to identical power absorption at any given sample dimension (N_w), except for a few N_w values for Group 2 materials beyond regime II. The overall magnitude of average power in Group 2 and Group 4 materials (high f_w) are less compared to Group 1 and Group 3. At regime I, it is observed that lateral and radial irradiations show similar power absorption for all groups of food materials. Regime II ($N_w \approx 0.7$) corresponds to higher power absorption with lateral irradiations compared to radial irradiations. At sample dimensions corresponding to regime III, it is observed that lateral and radial irradiations show similar magnitudes of absorbed power in Group 1 material while lateral irradiations show higher absorbed power for other groups of food (Groups 2-4). Regime I is characterized by the occurrence of single maxima for both lateral and radially irradiated food samples of Groups 1-4 with circular, Type 1 and Type 2 cross-sections. Multiple resonances (maxima) in power become prominent at sample dimensions greater than regime I ($N_w \approx 0.2$) for lateral irradiation and greater than regime II for radial irradiation all the three cross-sections.

Thermal runaway within food materials becomes

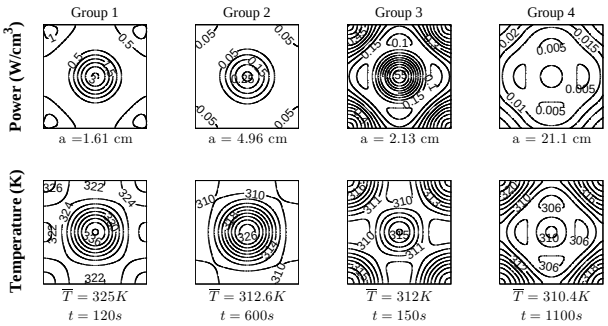

Figure 8b: Power and temperature profiles for food materials from Group 1-4 at sample radius corresponding to regime III for radially irradiated square (Type 1 or Type 2) samples.

significant for all the three cross-sections beyond regime I and it is observed that lateral irradiations result in larger thermal runaway compared to radial irradiations while former correspond to larger heating rates. In general, Type 2 configurations may not be recommended due to focussing of microwave power at the corners, which leads to larger thermal runaway compared to circle and Type 1. Based on overall heating rates, any of the configurations (circle, Type 1 or Type 2) with identical area may be recommended for all groups of food. However, Type 2 configurations at regime II and both Type 1 and Type 2 at regime III exhibit focussing of microwave power at certain corner points leading to higher temperatures along these corners which may be useful for targeted/selective heating along the corners. In regime I, either lateral or radial irradiations may be recommended for efficient processing while in other regimes, the choice between lateral and radial is based on factors such as heating rate, selective heating and thermal runaway.

References

[1] Oliveira, M. E. C., and Franca, A. S., Finite element analysis of microwave heating of solid products, International Communications in Heat and Mass Transfer, vol. 27, 2000, pp. 527-536.

[2] Hossan, M. R., Byun, D., and Dutta, P., Analysis of microwave heating for cylindrical shaped objects, International Journal of Heat and Mass Transfer, vol. 53, 2010, pp. 5129-5138.

[3] Bantle, M., Kafer, T., and Eikevik, T.M., Model and process simulation of microwave assisted convective drying of clipfish, Applied Thermal Engineering, vol. 59, 2013, pp. 675-682.

[4] Hossan, M.R., Dutta, P., Effects of temperature dependent properties in electromagnetic heating, International Journal of Heat and Mass Transfer, vol. 55, 2012, pp. 3412-3422.

[5] Sensoy, I., Sahin, S., Sumnu, G., Microwave Frying Compared with Conventional Frying via Numerical Simulation, Food and Bioprocess Technology, vol. 6, 2013, pp. 1414-1419.

[6] Chandrasekaran, S., Ramanathan, S., and Basak, T., Microwave food processing-a review, Food Research International, vol. 52, 2013, pp. 243-261.

[7] Vadivambal, R., and Jayas, D. S., Non-uniform temperature distribution during microwave heating of food materials-a review, Food and Bioprocess Technology., vol. 3, 2010, pp. 161-171.

[8] Chandrasekaran, S., Ramanathan, S., and Basak, T., Microwave material processing-a review, AIChE Journal., vol. 58, 2012, pp. 330-363.

[9] Ayappa, K. G., Davis, H. T., Barringer, S. A., and Davis, E. A., Resonant microwave power absorption in slabs and cylinders, AIChE Journal, vol. 43, 1997, pp. 615-624.

[10] Oliveira, M. E. C. and Franca, A. S., Microwave heating of foodstuffs, Journal of Food Engineering, vol. 53, 2002, pp. 347-359.

[11] Basak, T., Role of lateral and radial irradiations on efficient microwave processing of food cylinders, Chemical Engineering Science, vol. 62, 2007, pp. 3185-3196.

[12] Basak, T., Theoretical analysis on efficient microwave heating of materials with various square cross sections in the presence of lateral and radial irradiation, Journal of Physics D-Applied Physics, vol. 41, 2008, article number: 045405.

[13] Bhattacharya, M., and Basak, T., A novel closed-form analysis on asymptotes and resonances of microwave power, Chemical Engineering Science, vol. 61 , 2006a, pp. 6273-6301

[14] Bhattacharya, M., and Basak, T., On the analysis of microwave power and heating characteristics for food processing: Asymptotes and resonances, Food Research International, vol. 39, 2006b, pp. 1046-1057.

[15] Venkatesh, M. S., and Raghavan, G. S. V., An overview of microwave processing and dielectric properties of agri-food materials, Biosystems Engineering, vol. 88, 2004, pp. 1-18.

[16] Sosa-Morales, M. E., Valerio-Junco, L., Lopez-Malo, A., and Garcia, H. S., Dielectric properties of foods: Reported data in the 21st Century and their potential applications, LWT-Food Science and Technology, vol. 43, 2010, pp. 1169-1179.

[17] Zhang, L., Lyng, J. G., Brunton, N., Morgan, D., and McKenna, B., Dielectric and thermophysical properties of meat batters over a temperature range of 5-85°C, Meat Science, vol. 68, 2004, pp. 173-184.

[18] Ayappa, K. G., Davis, H. T., Crapiste, G., Davis, E. A., and Gordon, J., Microwave heating: An evaluation of power formulations, Chemical Engineering Science, vol. 46, 1991, pp. 1005-1016

[19] Wang, Y. F., Wig, T. D., Tang, J. M., and Hallberg, L. M., Dielectric properties of foods relevant to RF and microwave pasteurization and sterilization, Journal of Food Engineering, vol. 57, 2003, pp. 257-268.

[20] Boukouvalas, C. J., Krokida, M. K., Maroulis, Z. B., and Marinos-Kouris, D., Density and porosity: Literature data compilation for foodstuffs, International Journal of Food Properties, vol. 9, 2006, pp. 715-746.

[21] Polley, S. L., Snyder, O. P., and Kotnour, P. A Compilation of Thermal-Properties of Foods. Food Technology, vol. 34, 1980, pp. 76-&.

[22] Basak, T., and Rao, B. S., Role of ceramic composites and microwave pulsing on efficient microwave processing of pork meat samples, Food Research International, vol. 44, 2011, pp. 2679-2697

[23] Nuts and walnuts and black and dried density in 285 measurement units, `http://www.aqua-calc.com/page/density-table/substance/nuts,walnuts,dried//`, 2005.

[24] ASHRAE, 2006, chapter 9. Thermal properties of food.

[25] Plange, A. B., Addo, A., Kumi, F., and Piegu, A. K., Some moisture dependent thermal properties of cashew kernel, Australian Journal of Agricultural Engineering., vol. 3, 2012, pp. 6569.

[26] Stroshine, R. L., Physical properties of agricultural materials and food products, 2004.